

LA-UR-16-23636

Approved for public release; distribution is unlimited.

Title: Verification test of the SURF and SURFplus models in xRage

Author(s): Menikoff, Ralph

Intended for: Report

Issued: 2016-05-23



VERIFICATION TEST OF THE SURF AND SURFPLUS MODELS IN XRAGE

RALPH MENIKOFF

May 18, 2016

Abstract

As a verification test of the SURF and SURFplus models in the xRage code we use a propagating underdriven detonation wave in 1-D. This is about the only test cases for which an accurate solution can be determined based on the theoretical structure of the solution. The solution consists of a steady ZND reaction zone profile joined with a scale invariant rarefaction or Taylor wave and followed by a constant state. The end of the reaction profile and the head of the rarefaction coincide with the sonic CJ state of the detonation wave. The constant state is required to match a rigid wall boundary condition. For a test case, we use PBX 9502 with the same EOS and burn rate as previously used to test the shock detector algorithm utilized by the SURF model. The detonation wave is propagated for $10\,\mu\mathrm{s}$ (slightly under 80 mm). As expected, the pointwise errors are largest in the neighborhood of discontinuities; pressure discontinuity at the lead shock front and pressure derivative discontinuities at the head and tail of the rarefaction. As a quantitative measure of the overall accuracy, the L₂ norm of the difference of the numerical pressure and the exact solution is used. Results are presented for simulations using both a uniform grid and an adaptive grid that refines the reaction zone.

1 Introduction

It is desirable for a verification test to have an analytic solution to compare with a numerical solution. For an HE model with realistic equations of state (EOS), there are no known analytic solutions. However, for a 1-D propagating underdriven detonation wave, there is a semi-analytic solution based on the theoretical structure of the solution — a steady ZND detonation wave profile (lead shock followed by a reaction zone) joined with a scale invariant rarefaction (known as a Taylor wave), and followed by a constant state; see for example ref. [Fickett and Davis, 1979, § 2C]. The end of the reaction profile and the head of the rarefaction coincide at a sonic point, the CJ detonation state. The constant state is required to match a rigid wall boundary condition. The solution can be determined by solving algebraic equations for the partly burned detonation loci, an ODE for the reaction progress variable, and another ODE for the isentrope from the CJ state. The semi-analytic solution can be computed sufficiently accurate to serve as an 'exact' solution for verification tests. The solution method we use is based on the formulation in ref. [Menikoff, 2015].

Here we use an underdriven detonation wave as a verification test of the SURF and SURFplus models as implemented in the Eulerian hydro code xRage. The SURF model [Menikoff and Shaw, 2010] is based on the ignition and growth concept of hot spots in a heterogeneous HE [Lee and Tarver, 1980]. The SURFplus model [Menikoff and Shaw, 2012] is an extension that adds a second slow reaction for the energy release from carbon clustering. A novel feature of the SURF model is that the burn rate depends on the lead shock pressure. The current formulation of these models are described in [Menikoff, 2016, App. A & B].

This report is a follow on to the previous work investigating the shock detector algorithm utilized for the SURF model burn rate. The aim here is to be more quantitative by comparing a numerical solution with an exact solution. The test case simulations are for PBX 9502 with the same EOS and burn rate as in the report on the shock detector [Menikoff, 2016, App. C & D].

2 Test problem

Simulations utilize a 100 mm mesh with a wall boundary on the left. The initial pressure profile of the underdriven detonation wave for the SURF and SURFplus models are shown in fig. 1. The front is at x = 10 mm, and the Taylor wave corresponds to a centered rarefaction after its head has propagated 5 mm. The rarefaction ends with a particle velocity of zero and is followed by a constant state.

The pointwise relative error shown in fig. 1 for a fine uniform grid and an adaptive grid is a check on the initialization utilizing the exact solution in tabular form. The solution table was

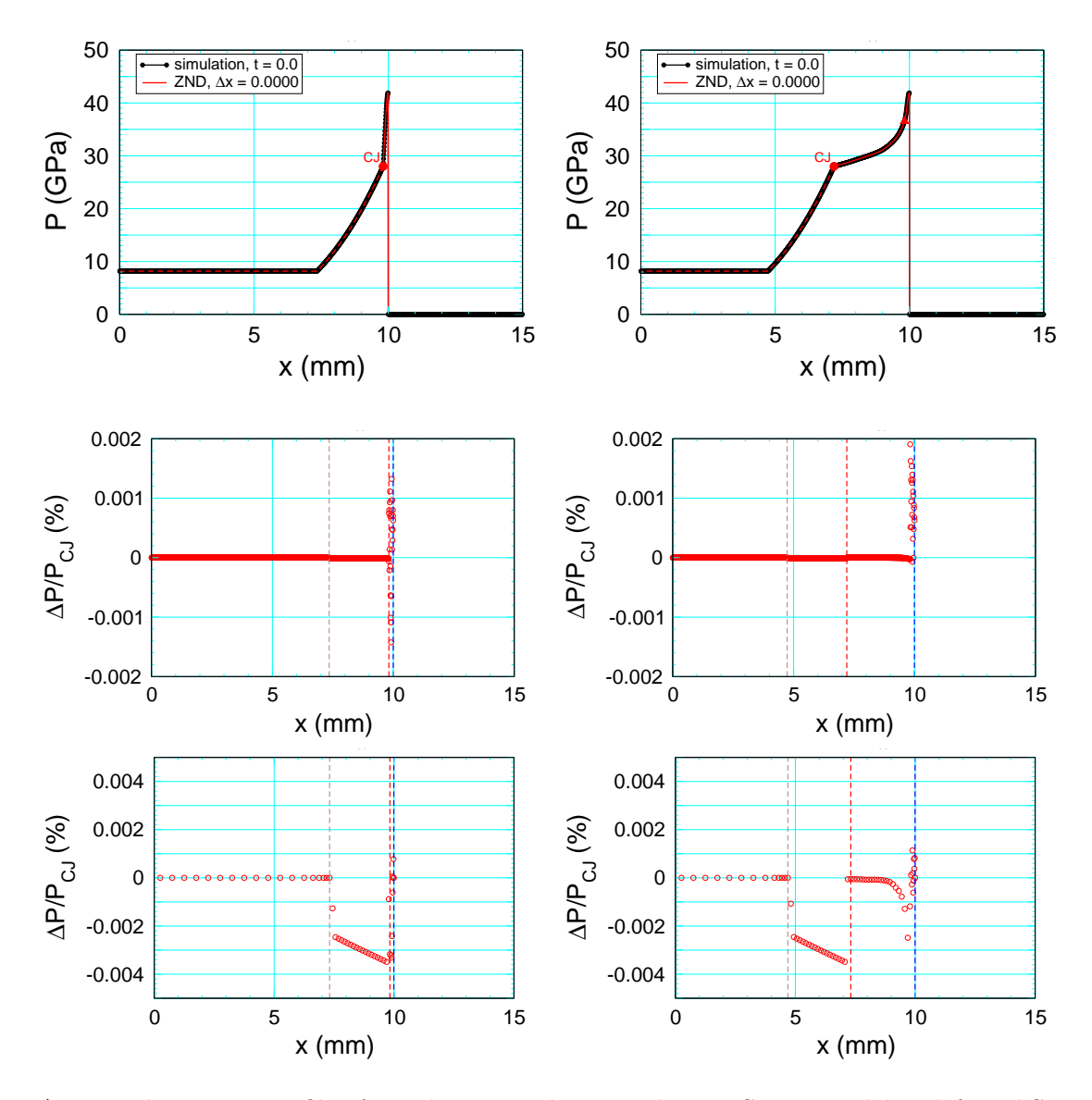


Figure 1: Initial pressure profile of simulations and exact solution; SURF model on left and SURFplus model on right. Top plots are pressure, middle plots are relative error, $(P - P_e)/P_{\rm CJ}$ for fine uniform grid, and bottom plots are relative error for adaptive grid with coarser zones in the Taylor wave. Symbols denote values at cell centers. The label 'CJ' indicates the end of the reaction zone/head of the rarefaction wave. The red triangle on the SURFplus plot indicates the end of the fast reaction. On the error plots, the dashed blue, red and brown vertical lines denote the detonation front, and the head and tail of the rarefaction, respectively.

generated by an external routine utilizing the equivalent HE model (EOS and burn rate) as used for the **xRage** simulations. To minimize interpolation errors, the table is constructed to have grid points at the cell centers of the computational mesh. By including the sound speed in the solution table, the exact solution at later times can be determined from the table.

The small discrepancy in the initial reaction zone pressure results from an interpolation error due to xRage calculating the P-T equilibrium EOS of partly burned HE using tabular EOS for the reactants and products. The interpolation error is minimized (< 0.002%) by using EOS tables with a fine grid; 120 points per decade in pressure and 40 points per decade in temperature.

For the Taylor wave and the portion of the reaction zone after the fast (SURF) reaction for the SURFplus model, the analytic EOS for the products is used. The small discrepancy in the pressure for the products is due to the way in which the specific internal energy is calculated for the evaluation of the pressure, P(V, e). The xRage code stores and updates conserved variables; the cell mass (M), cell momentum (P) and the total cell energy (E). The internal energy is e = (E - KE)/M. For the average cell kinetic energy, the velocity is taken to be linear. Hence, there is a small difference with the initialization that is based on the specific internal energy e at the center of the cell. The energy difference scales with cube of the cell size. This gives rise to an error in relative pressure which is insignificant for the small cell size $(\Delta x = 0.0078 \, \text{mm})$ of the fine uniform mesh, and small but noticeable $(< 0.004 \, \%)$ for the amr mesh with $\Delta x = 0.125 \, \text{mm}$ in the Taylor wave.

2.1 Overview

The time evolution of the solution is shown in fig. 2. The solution in the rest frame of the detonation front clearly shows that the reaction zone is steady and the Taylor wave spreads out in time. We note that the constant state region grows in extent since the characteristic speed (u+c) at the tail of the rarefaction wave is positive. Other then setting the pressure of the constant state, the wall boundary does not affect the flow.

The CJ state and the lead shock state are the same for the SURF and SURFplus models. An important difference between the models is the width of the reaction zone. This affects the magnitude of the kink in the pressure profile or discontinuity of the pressure derivative at the end of the reaction zone and the head of the rarefaction. At the end of the simulation, the kink is small and barely noticeable for the SURFplus model, while it is large and significant for the SURF model.

Later we will see that the numerical smearing of the kink affects the position of the sonic point relative to the end of the reaction zone. The reaction zone is acoustically decoupled from

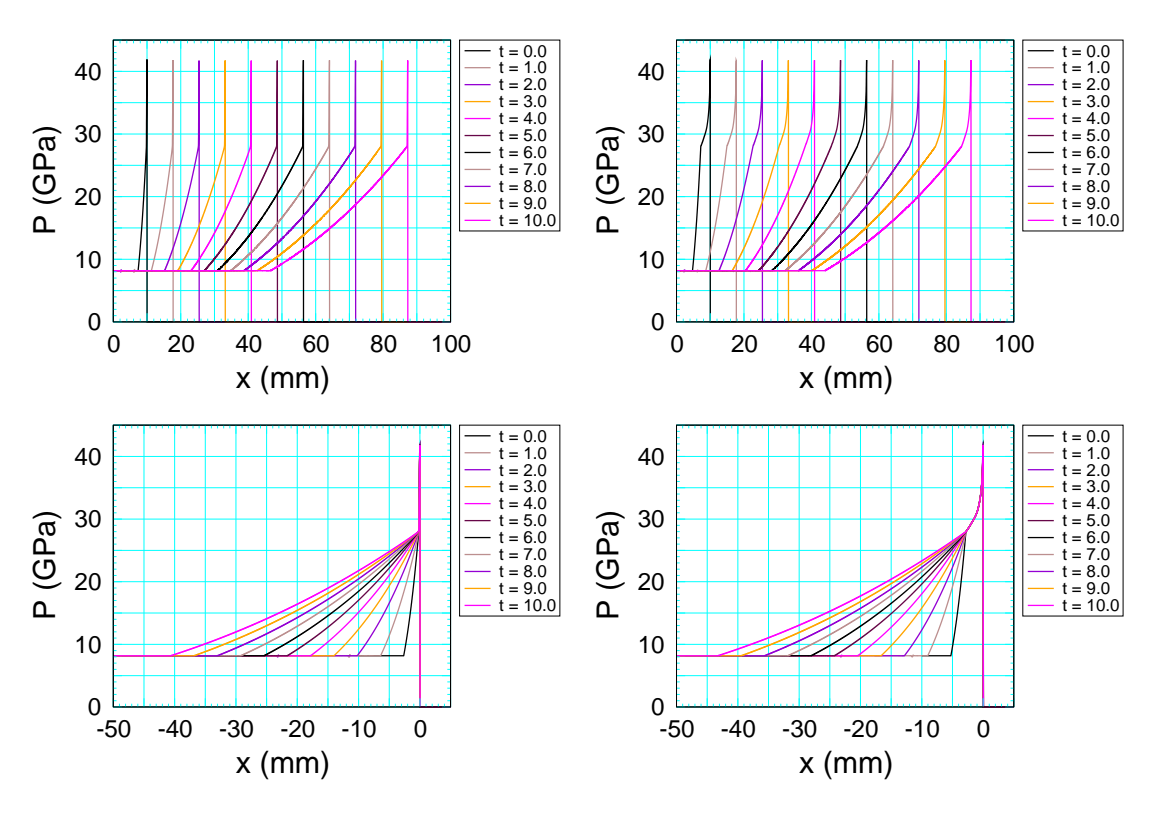


Figure 2: Time evolution of pressure profiles; SURF model on left and SURFplus model on right. Top plot is in lab frame and bottom plot is in rest frame of the detonation front.

the flow to the left of the sonic point. Errors in the lead shock pressure from the shock detector algorithm give rise to numerical fluctuations within the reaction zone. These can be a source of acoustic noise propagating along the left characteristic through the sonic point and into the rarefaction wave; i.e., sonic point (D = u + c) is with respect to only right facing acoustic waves.

2.2 Metric for comparison

To quantify the comparison between a numerical solution and the exact solution, we use a numerical approximation of the L_2 -norm of the pressure difference,

$$||P - P_e||^2 = \frac{\sum_{i=1}^{N-1} \left(\frac{1}{2} \left[P_i + P_{i+1}\right] - \frac{1}{2} \left[P_e(x_i - \Delta x, t) + P_e(x_{i+1} - \Delta x, t)\right]\right)^2 \left(x_{i+1} - x_i\right)}{x_N - x_1}, \quad (1)$$

where P_i is the numerical solution at the center of the i^{th} cell at time t, and $P_e(x_i - \Delta x, t)$ is the

corresponding exact solution. For an adaptive grid the norm corresponds to a cell size weighted average of the root-mean squared error of the pressure at the cell centers.

The exact solution is shifted in space by Δx such that the average of the pressure difference is 0. This enables the smeared out numerical shock front to be aligned with the discontinuous shock front of the exact solution. The time variation of the shift can be associated with a slight variation or error in the numerical detonation speed. By choosing N such that P_N is the peak pressure, the norm excludes the error from the numerical shock profile including any burn that occurs in the shock profile.

The detonation pressure, *i.e.*, pressure at the end of the reaction zone denoted by P_{CJ} , is the natural pressure scale. Therefore, as a measure of the relative error of the numerical solution, we use $||P - P_e||/P_{\text{CJ}}$.

3 Numerical results

Simulations were run with a uniform fine grid and with an adaptive mesh refinement (amr) grid. The fine grid had 128 cells per mm (cell size of 0.0078 mm), which gives 25 cells in the portion of reaction zone with the fast (SURF) rate.

The amr grid had 64 cells per mm (cell size of 0.0156 mm) in the fast (SURF) rate portion of the reaction zone, up to 8 cells per mm (cell size of 0.125 mm) to resolve pressure gradients in the slow (SURFplus) rate portion of the reaction zone and the steep part of Taylor wave, down to 0.5 mm for the constant state region.

Typical zoning used for applications is much coarser for the fast (SURF) rate (10 to 20 cells per mm) and similar to the amr grid (up to 8 cells per mm) for the slow (SURFplus) rate and the Taylor wave. With the coarser zoning, there are only 2 to 4 cells in the fast (SURF) portion of the reaction zone. Effectively, the detonation wave is captured rather than resolved. In 1-D, there is no curvature effect. The CJ detonation state is determined by the shock jump conditions, and is independent of the burn rate. Hence, resolving the reaction zone is not crucial for the detonation speed and the Taylor wave.

3.1 Uniform fine grid

The pressure profiles and pointwise errors in the reaction zone at a sequence of times are shown for the SURF model in fig. 3 and for the SURFplus model in fig. 4. Several features are noteworthy:

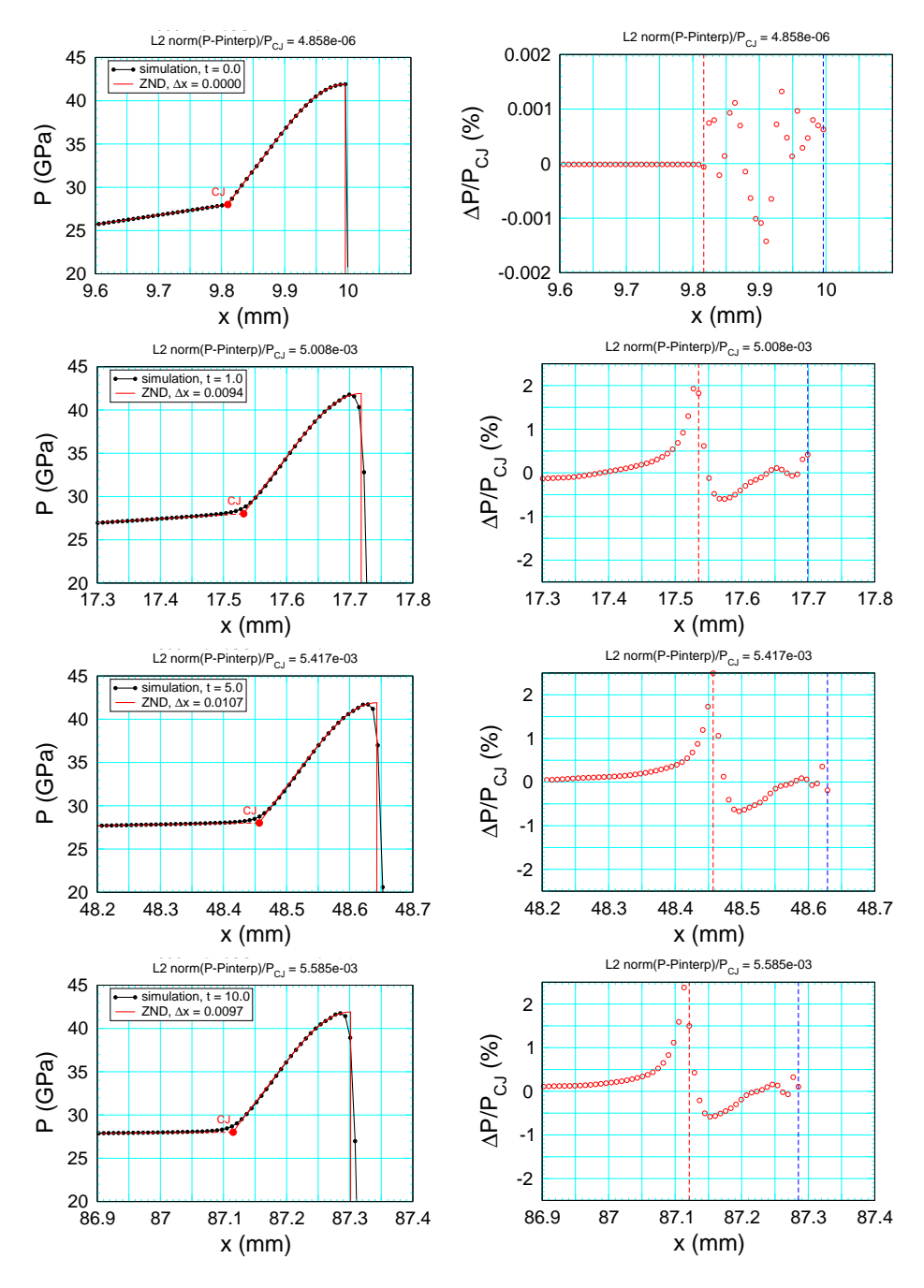


Figure 3: Comparison of reaction zone pressure profile with exact solution for SURF model simulations on uniform fine mesh. Left plots are pressure profile and right plots are relative pointwise error. Top to bottom is sequence of times. Symbols denote values at cell centers.

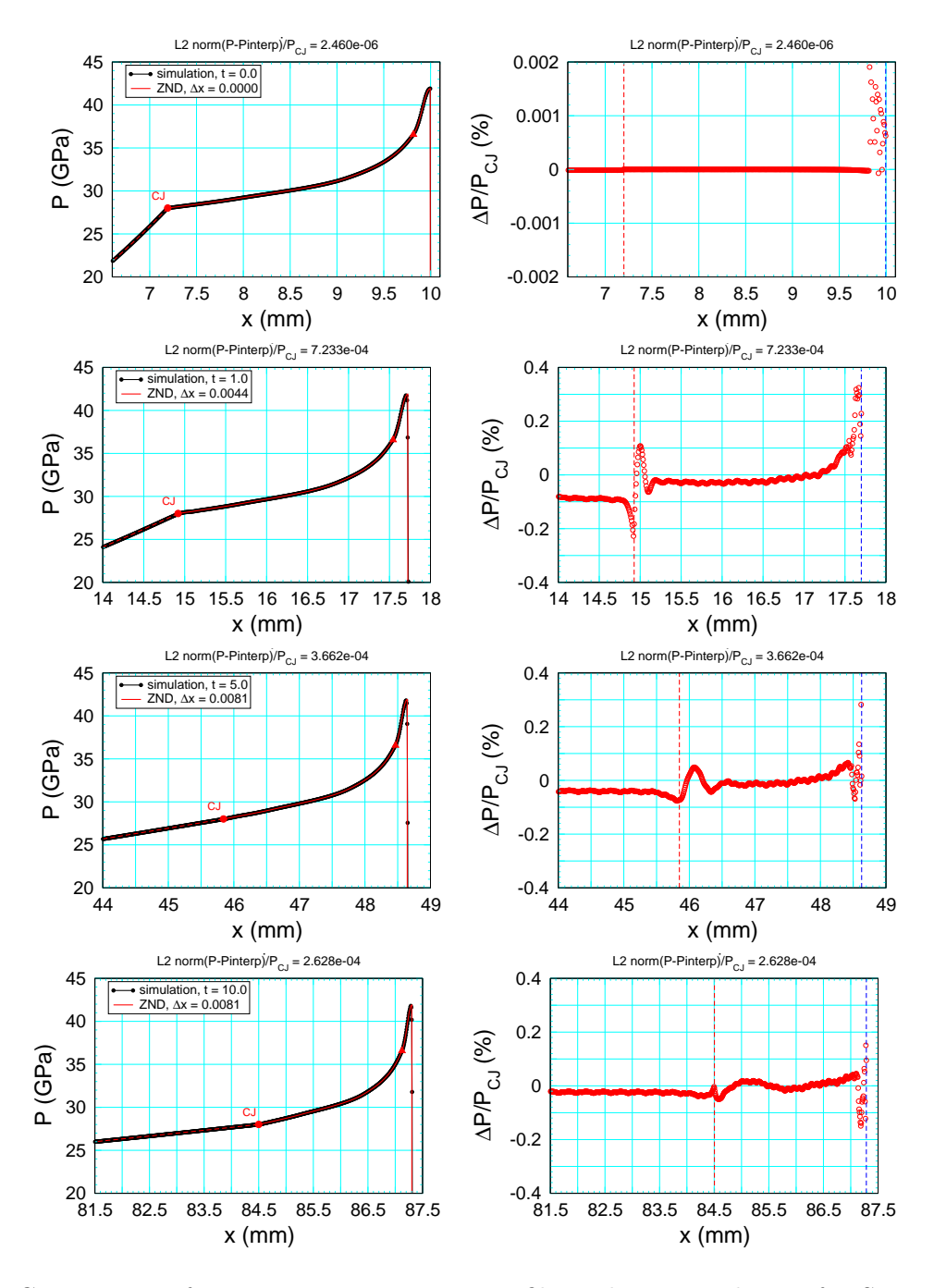


Figure 4: Comparison of reaction zone pressure profile with exact solution for SURFplus model simulations on uniform fine mesh. Left plots are pressure profile and right plots are relative pointwise error. Top to bottom is sequence of times. Symbols denote values at cell centers.

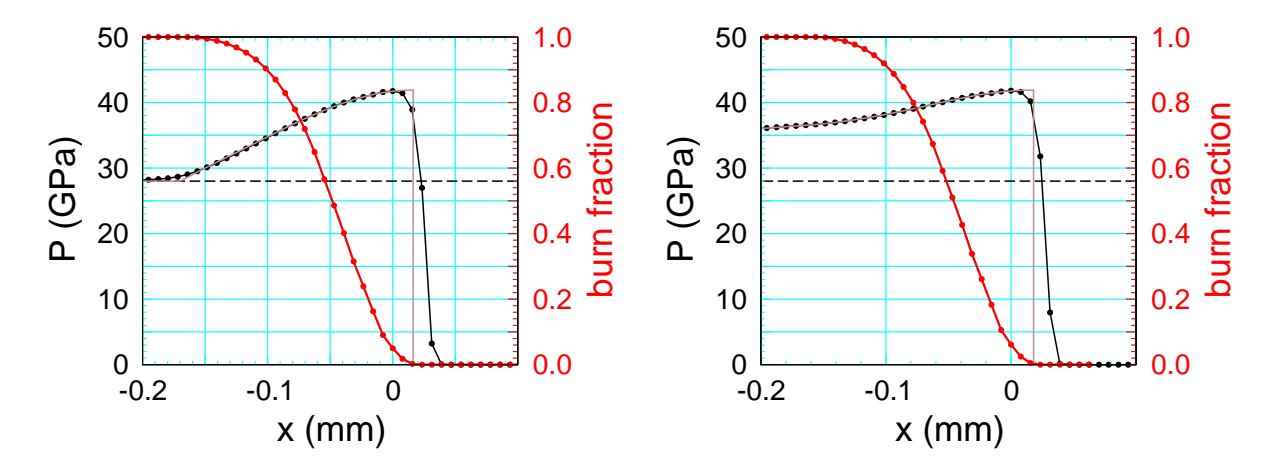


Figure 5: Profiles of pressure and burn fraction for fast (SURF) reaction at the end of run for simulations with uniform fine grid. SURF model simulation on left and SURFplus model simulation on right. Brown curve is exact solution. Dashed black line is CJ pressure. Symbols denote values at cell centers. Spatial coordinate is relative to peak pressure.

- 1. The pointwise error in the initialization (t=0) is small compared to the error at later time. After t=0, the lead shock is smeared out and the numerical and the exact shock fronts need to be aligned. As seen in fig. 5, the shift, Δx in Eq. (1), is 1 to 2 times the cell size, which is about half the shock width. There is a few per cent burn in the numerical shock rise. The shift accounts for most of the burning in the shock profile. Since the shock jump conditions apply to partly burned HE, the burning in the shock rise has a small effect on the profile behind the front. Moreover, the shock width is a fixed number of cells. With a smaller cell size the shock rise time would decrease, and hence the burning in the shock profile would decrease.
- 2. The spatial shift to align the lead shock front, greatly reduces the pointwise error in the reaction zone. However, as shown in fig. 6, it does increase the pointwise error in the Taylor wave. The red error band results from a short wave length oscillation. The oscillation is due to acoustic noise generated by fluctuation in the reaction zone and propagated upstream along the left characteristic. The amplitude is small, $\pm 0.01\%$. A running average (black curve) over 41 points $(0.320\,\mathrm{mm})$ greatly reduces the oscillations. The fast (SURF) reaction zone width is 25 cells. Hence, the length scale for the average is 64% larger than the reaction zone width $(0.195\,\mathrm{mm})$. The slope of the average error in the rarefaction wave is mostly due to the spatial shift in the pressure profile. The net result of the shift, decreasing the pointwise error in the reaction zone and increasing it in the Taylor wave, is to decrease the metric for the average error by about a factor of 3.

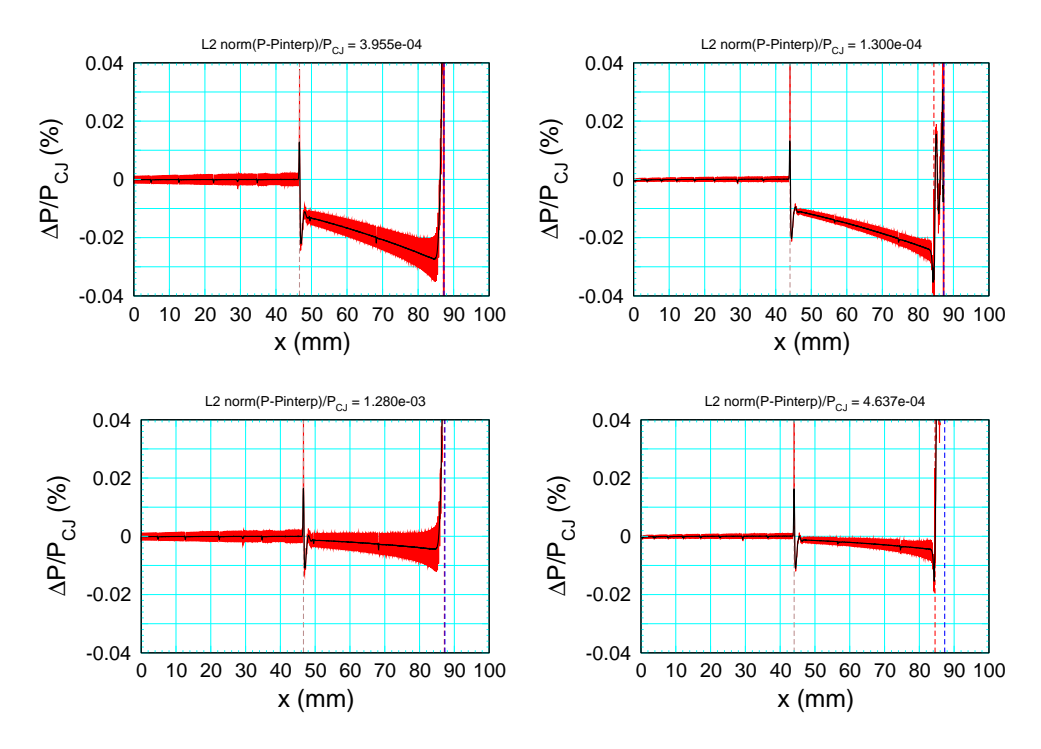


Figure 6: Profiles of pointwise pressure error at end of run for simulations with uniform fine grid. SURF model simulation on left and SURFplus model simulation on right. Top plots with shift to align shock front, and bottom plots without shift. Black curve is running average over 41 points.

3. A large pointwise error occurs at the sonic point. It is associated with the numerical smearing of the kink; *i.e.*, the discontinuity in the pressure derivative between the end of the reaction zone and the head of the rarefaction wave. Due to the difference in the reaction zone widths, the slope of the pressure profile at the end of the reaction zone differs between the SURF and SURFplus models. This affects the magnitude of the kink in the pressure profile. In addition, the magnitude of the kink changes as the flow evolves due to the spreading out of the rarefaction wave, which decreases the pressure derivative. At the end of the simulation, the kink is smaller for the wide reaction zone of the SURFplus model, and the pointwise error in the vicinity of the sonic point is also smaller for the SURFplus model. Similarly, a large pointwise error occurs for the kink at the tail of the rarefaction wave; see fig. 6. The kink at the tail is independent of the reaction model and the pointwise error is the same.

The sonic point plays a critical role in an underdriven detonation wave as it determines the detonation speed and the state behind the detonation wave. Profiles of the pressure, reaction progress variable and characteristic speed, in the vicinity of the sonic point are shown in fig. 7. The sonic point corresponds to the intersection of the curves for the detonation speed and the

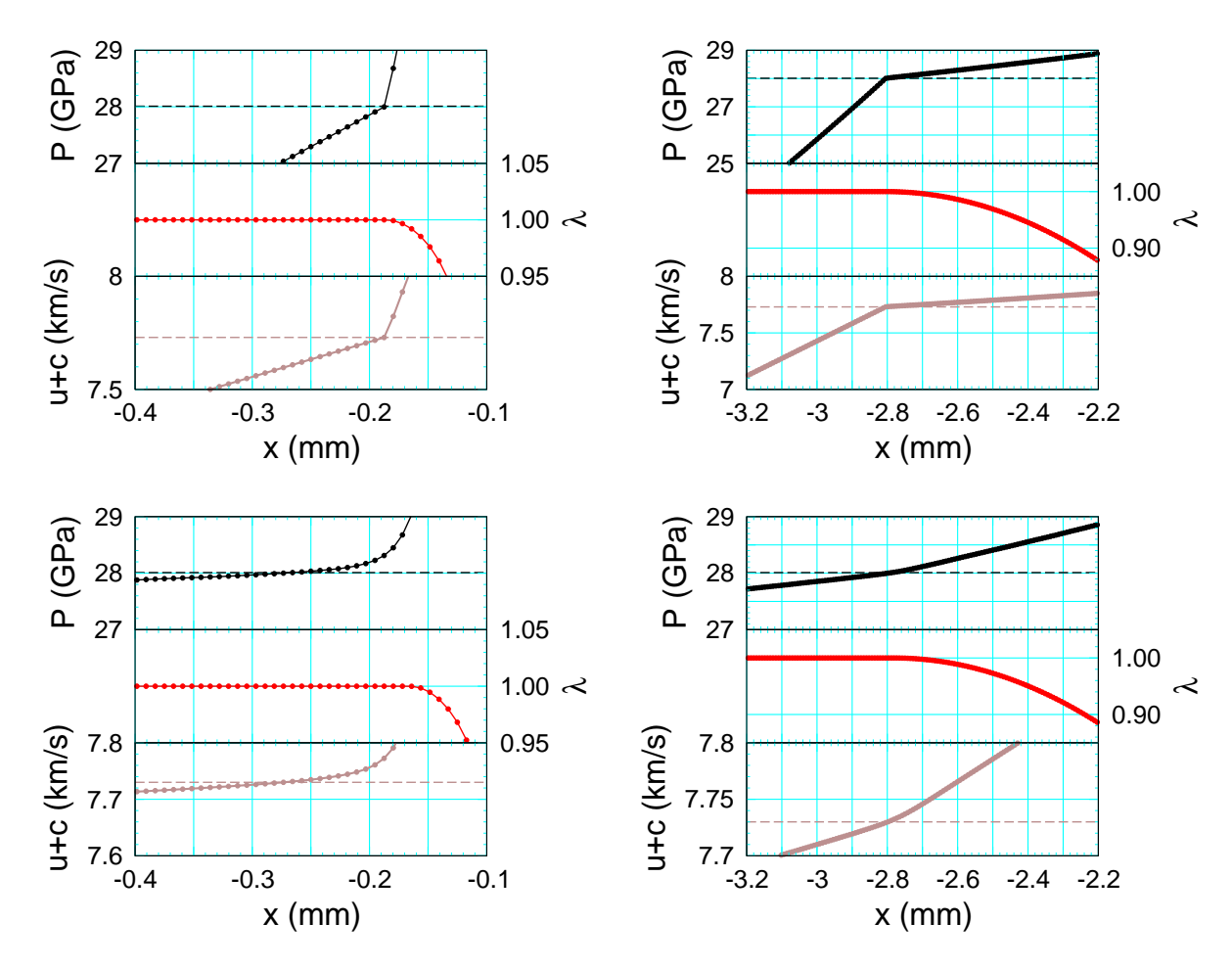


Figure 7: Profiles of pressure, reaction progress variable (λ) and characteristic speed (u+c) in the neighborhood of the sonic point for simulation on uniform fine mesh. Dashed black line is CJ pressure, and dashed brown line is detonation speed. Symbols denote values at cell centers of computational grid. Left plots for SURF model and right plots for SURFplus model. Top plots at t=0 and bottom plots at $t=10\,\mu\text{s}$. Sonic point (D=u+c) is at the intersection of solid and dashed brown curves. End of the reaction zone is the point with the largest x and $\lambda=1$. Spatial distance is relative to detonation front (peak pressure).

characteristic velocity (u+c). For the exact solution it occurs at the end of the reaction zone $(\lambda = 1)$ and the sonic state has the CJ pressure. This is seen in the initial t = 0 profiles.

At the end of the simulation ($t = 10 \,\mu\text{s}$), the numerical smearing of the pressure profile at the sonic point kink affects these properties. With the SURF model, the kink is large and the sonic point occurs noticeably behind the end of the reaction zone. The CJ pressure is within a

couple of cells of the sonic point. Despite the sonic point not occurring at the end of the reaction zone, there is no significant effect on either the detonation speed or the steady state nature of the reaction zone.

Remark: The xRage hydro algorithm is flux based and hence in conservative form. For conservative form, the shock jump conditions are expected to be satisfied for a steady wave. Since the CJ state lies on the detonation locus, it is surprising that the sonic point and the end of the reaction zone do not coincide. Very likely this is related to the fact that the CJ state is sonic, which gives rise to transonic flow (in the rest frame of the detonation front) and a kink in the pressure profile. The discrepancy between the end of the steady detonation wave profile and the jump conditions is quite significant for coarser resolution when the detonation wave is captured rather than having a resolved reaction zone profile. For a possible explanation of the discrepancy see [Menikoff, 2014, Appendic C].

The value of the metric for comparing the numerical pressure profile with the exact solution is listed in table 1 for a sequence of times. We note that after the initial smearing of the discontinuities at the shock front and the kinks at the head and tail of the rarefaction, the metric changes slowly. In addition, the metric is slightly lower for the SURFplus model than for SURF model. This is due to the smaller magnitude of the kink in the pressure profile at the sonic point.

We also note that the shift Δx to align the numerical and exact shock fronts is less than twice the cell size. This implies that the position of the front, and hence the detonation speed is accurate. The table also lists the reaction progress variable λ at the peak pressure, which roughly corresponds to the numerical shock front. The metric, Eq. (1), excludes the error from the numerical shock rise and the burning within the shock profile by only utilizing the profile up to the peak pressure.

Table 1: Pressure profile metric, Eq. (1), for simulations on uniform grid with 128 cells per mm.

	SURF			SURFplus		
time	Δx	$\lambda @ P_{max}$	$ P - P_e /P_{\text{CJ}}$	Δx	$\lambda@P_{max}$	$ P - P_e /P_{\text{CJ}} $
μs	mm	per cent		mm	per cent	
0	0.0	0.0	9.6e-7	0.0	0.0	1.4e-6
1	0.0094	6.5	1.3e-3	0.0043	7.7	7.3e-4
5	0.0107	4.0	5.6e-4	0.0081	5.3	2.2e-4
10	0.0097	5.0	4.0e-4	0.0081	6.1	1.3e-4

The SURF burn rate depends on the lead shock pressure. A significant source of error for the reaction zone is due to the fluctuations in the detected shock pressure. This was investigated in previous report [Menikoff, 2016]. For the simulation on the fine uniform fine mesh, the lead shock pressure is slightly low (0.2 out of 41.9 GPa) and has high frequency fluctuation of about ± 0.02 GPa. Because the burn rate asymptotes at high shock pressure, the relative error in the rate is less than the relative error in the shock pressure. Unless the offset in the lead shock pressure is compensated for in the 'exact solution', there will be a small minimum error in the reaction zone independent of resolution. Since the CJ state does not depend on the details of the reaction rate, the Taylor wave should not be affected by a systematic error in the burn rate.

3.2 AMR grid

The pressure profiles and pointwise errors in the reaction zone at a sequence of times is shown for the SURF model in fig. 8 and for the SURF plus model in fig. 9. Compared to the simulations on a uniform fine mesh we observe the following:

- 1. For the SURF model, the smearing at the sonic point kink leads to a pointwise error of similar magnitude.
- 2. For the SURFplus model, the smearing at the sonic point kink leads to a larger pointwise error than for the uniform grid. However, it less than that for the SURF model.
- 3. For the SURFplus model, amr cell size for slow rate portion of the reaction zone is considerably coarser than for the uniform fine mesh. The pointwise error is much larger for the coarse mesh.
- 4. The short-wavelength low-amplitude oscillations in Taylor wave observed with the fine zoning gets averaged out with coarser amr zoning; compare fig. 6 and fig. 10.

At the end of the run, the pressure profile with the burn fraction superimposed is shown in fig. 11. In the fast rate portion of the reaction zone, the amr cell size is twice that of the fine uniform mesh. Again the shift Δx needed to align the numerical shock front with the exact front is 1 to 2 times the cell size or about half the numerical shock width. However, there is considerably more burning at the peak pressure, which roughly corresponds to the numerical shock front.

Profiles of the pressure, reaction progress variable and characteristic speed, in the vicinity of the sonic point are shown in fig. 12. The zoning about the sonic point for the adaptive mesh is much coarser for the SURFplus model than for the SURF model. Moreover, the SURF model zoning is much coarser than for the uniform fine mesh. For both the adaptive mesh and the uniform mesh, the SURF model reaction ends before the sonic point by about the same spatial

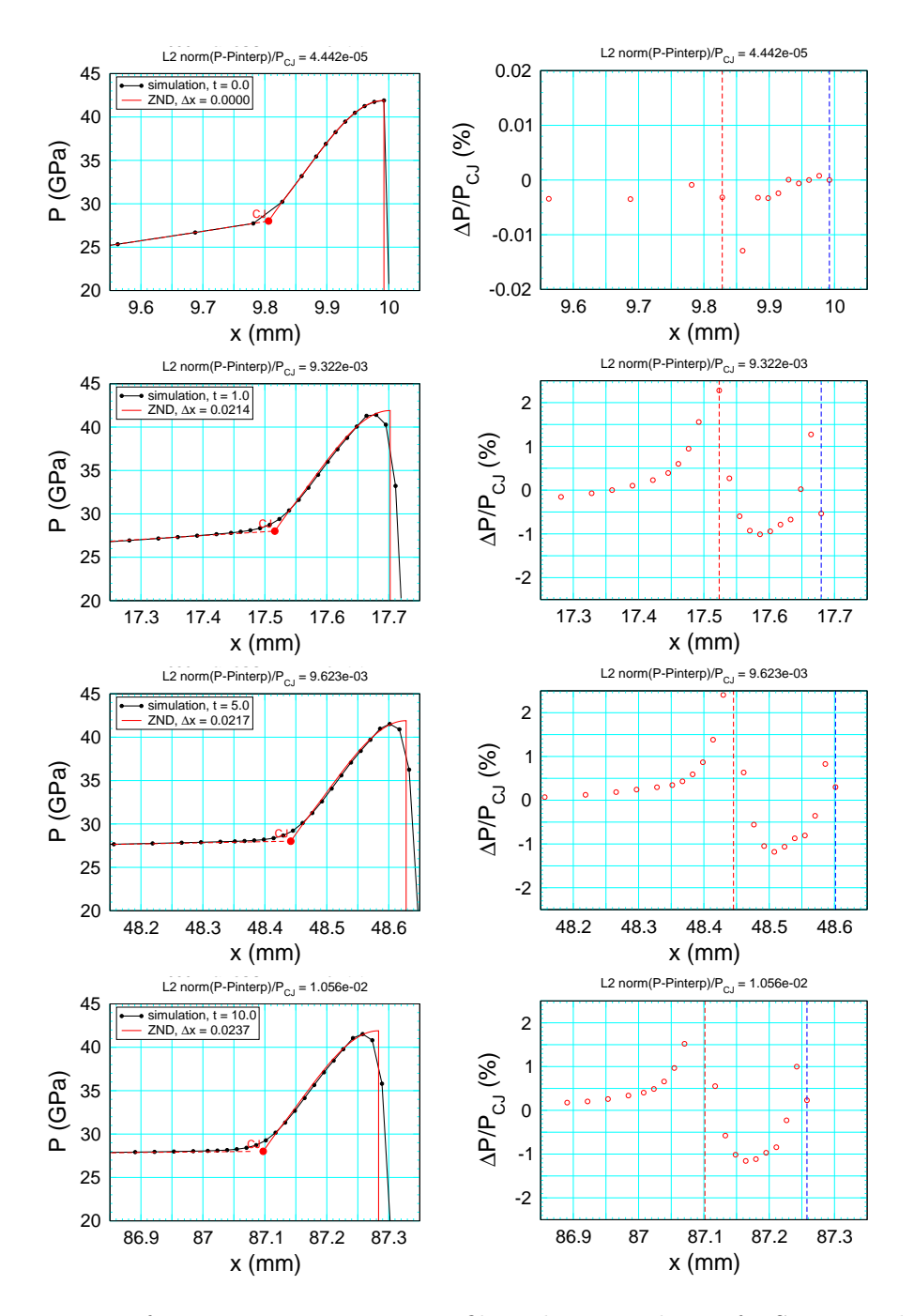


Figure 8: Comparison of reaction zone pressure profile with exact solution for SURF model simulations with an adaptive mesh. Left plots are pressure profile and right plots are relative pointwise error. Top to bottom is sequence of times. Symbols denote values at cell centers.

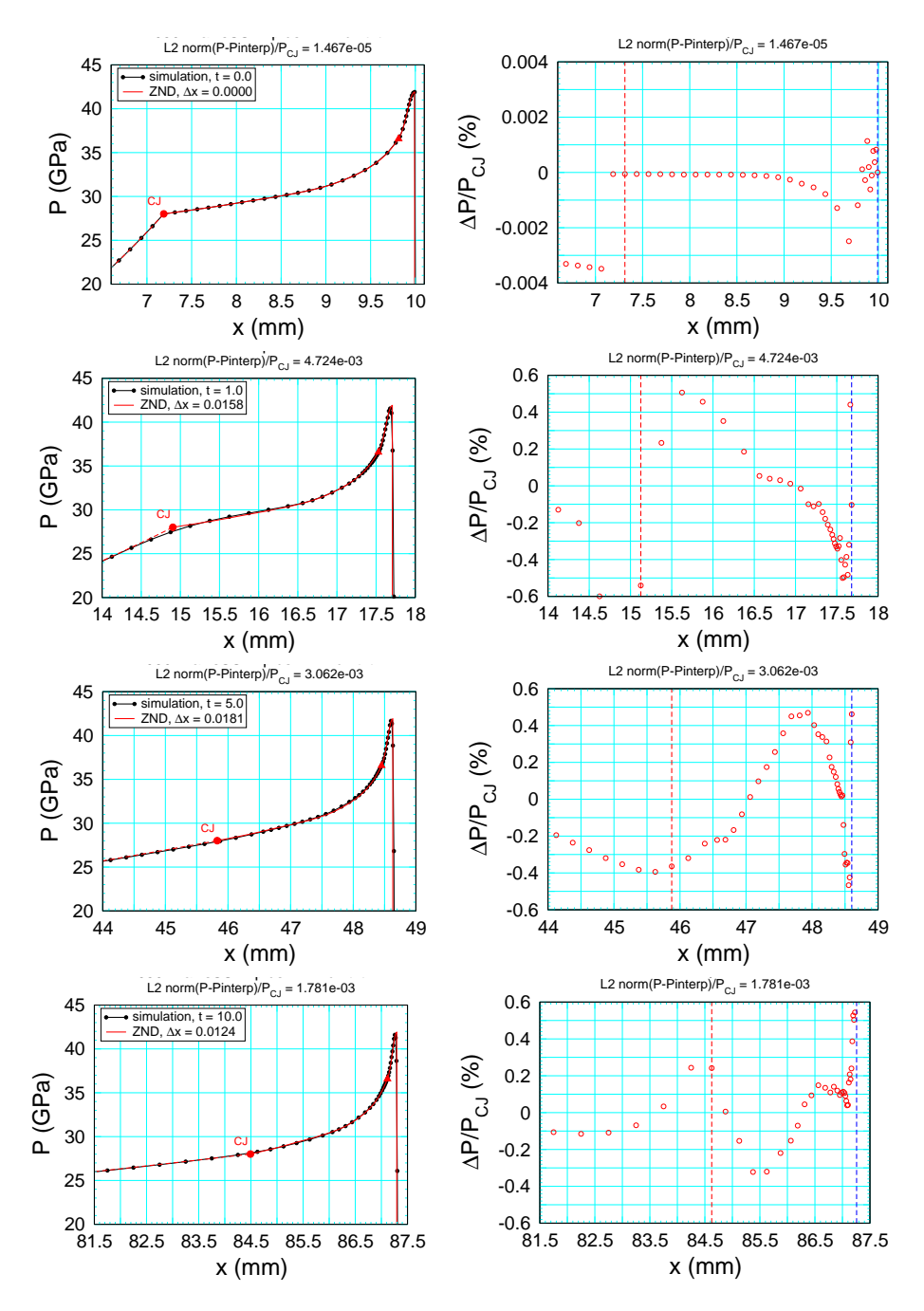
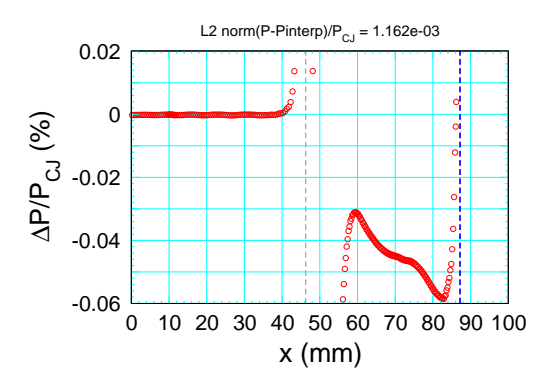
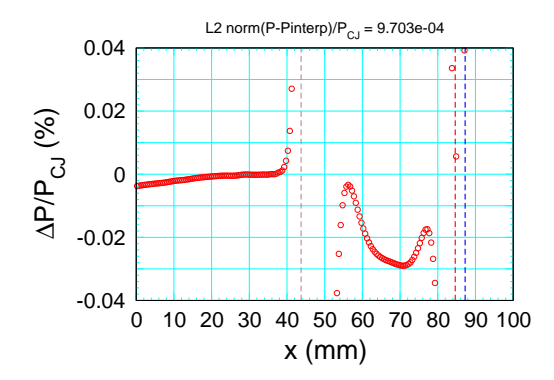


Figure 9: Comparison of reaction zone pressure profile with exact solution for SURFplus model simulations with an adaptive mesh. Left plots are pressure profile and right plots are relative pointwise error. Top to bottom is sequence of times. Symbols denote values at cell centers.





1.0

8.0

0.6

0.4

0.2

0.0

Figure 10: Profiles of pointwise pressure error at end of run for simulations with amr grid. SURF model simulation on left and SURF plus model simulation on right.

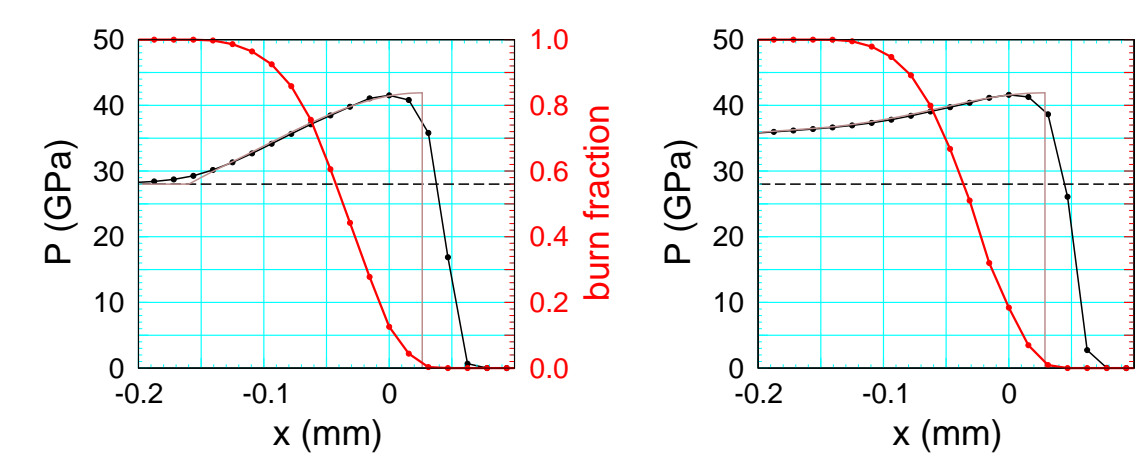


Figure 11: Profiles of pressure and burn fraction for fast (SURF) reaction at the end of the simulations with an adaptive mesh. SURF model simulation on left and SURFplus model simulation on right. Brown curve is exact solution. Dashed black line is CJ pressure. Symbols denote values at cell centers. Spatial coordinate is relative to peak pressure.

distance. For the SURFplus model, the end of the reaction zone is nearly the same as the sonic point. However, with the coarser adaptive mesh the reaction zone is slightly longer.

The value of the metric for comparing the numerical pressure profile with the exact solution is listed in table 2 for a sequence of times. The adaptive mesh metrics are about the same for both the SURF model and SURFplus model. Moreover, they are about a factor of 10 larger than those for the fine uniform grid. The increase in accuracy is computationally costly. The fine uniform mesh had slightly over 12 thousand cells, while the adaptive mesh had less than

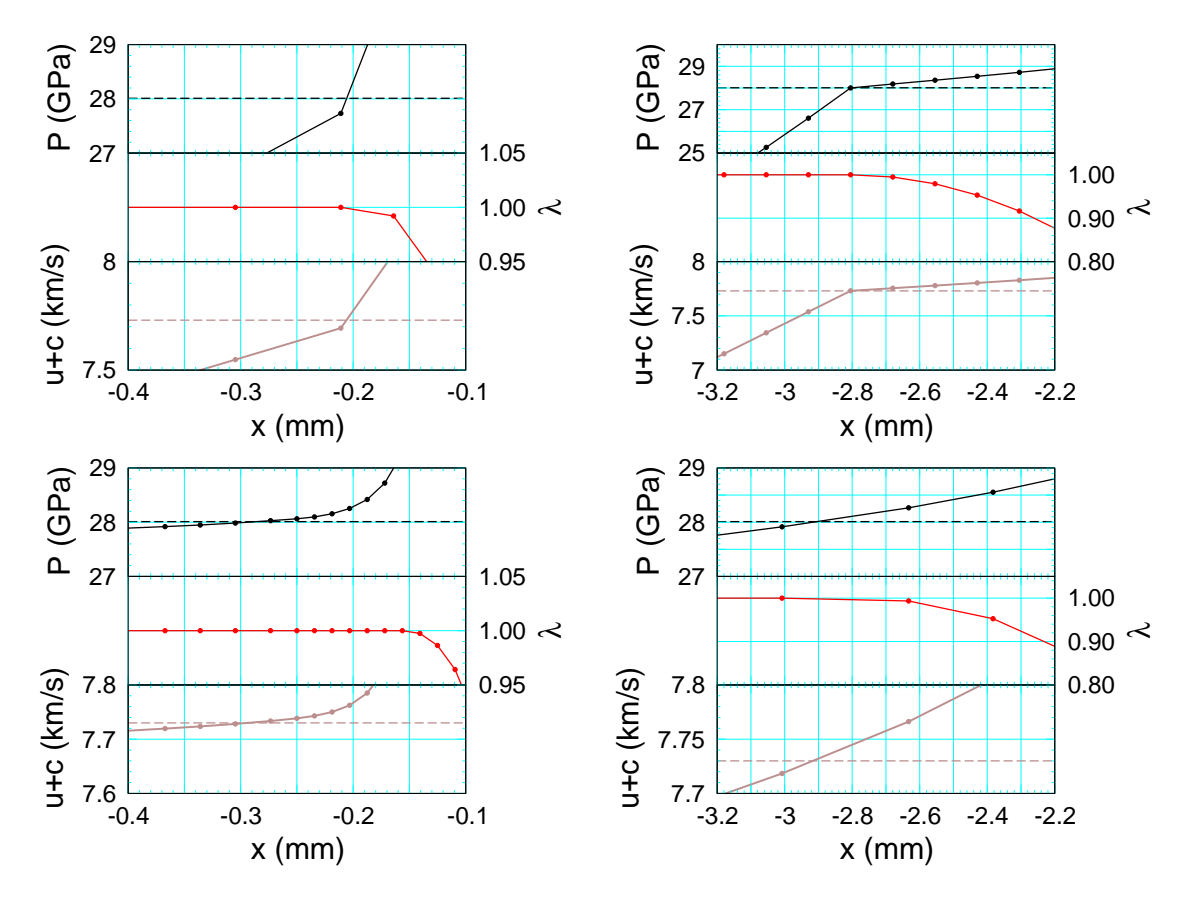


Figure 12: Profiles of pressure, reaction progress variable (λ) and characteristic speed (u+c) in the neighborhood of the sonic point for simulation with adaptive mesh. Dashed black line is CJ pressure, and dashed brown line is detonation speed. Symbols denote values at cell centers of computational grid. Left plots for SURF model and right plots for SURFplus model. Top plots at t=0 and bottom plots at $t=10\,\mu\mathrm{s}$. Sonic point (D=u+c) is at the intersection of solid and dashed brown curves. End of the reaction zone is the point with the largest x and $\lambda=1$. Spatial distance is relative to detonation front (peak pressure).

500 cells. On a single Xeon X5550 processor, the fine uniform mesh took 1.7 hours, while the adaptive mesh took only 0.1 hours.

Table 2: Pressure profile metric, Eq. (1), for simulations on an adaptive mesh.

	SURF			SURFplus		
time	Δx	$\lambda @P_{max}$	$ P - P_e /P_{\text{CJ}}$	Δx	$\lambda @ P_{max}$	$ P - P_e /P_{\text{CJ}} $
$\mu \mathrm{s}$	mm	per cent	_	mm	per cent	
0	0.0	0.0	1.6e-5	0.0	0.0	1.5e-5
1	0.0214	9.7	2.3e-3	0.0158	14.9	2.6e-3
5	0.0217	12.7	1.6e-3	0.0181	18.5	1.6e-3
10	0.0237	12.6	1.2e-3	0.0124	18.4	1.0e-3

4 Summary

Compared to the exact solution, numerical solutions for propagating a detonation wave smear out discontinuities. The largest pointwise errors in the pressure profile occurs at the shock front, and the head and tail of the rarefaction. For a uniform grid with 128 cells/mm, at the end of the reaction zone/head of the rarefaction, the relative pointwise error is about 2.5% for the SURF model, but less than 0.1% for the SURF plus model. The smaller value for the SURF plus model is due to the smaller magnitude of the kink (discontinuity in the pressure derivative) which results from the larger reaction zone width of the second slow reaction. The average error as measured by the L₂-norm of the pressure difference (0.04%) is smaller than the largest pointwise error by a significant factor. With an adaptive mesh the L₂-norm is somewhat larger (0.2%) but much less computationally expensive in terms of both memory usage and computer time.

A general property of an underdriven detonation wave is that the end of the reaction zone is a sonic point (D = u + c). The sonic point gives rise to a kink in the pressure profile. The numerical smearing of the kink causes the sonic point to occur after the sonic point. The spatial discrepancy is significant for the SURF model but small for the SURF plus model. Again this is due to the difference in the magnitude of the kink resulting from the width of the reaction zone.

Most important for applications are the detonation speed and the pressure on the release isentrope from the end of the reaction zone. The errors in these quantities are much smaller than the pointwise error in the neighborhood of the sonic point, despite the theoretical significance of the sonic point determining the underdriven detonation wave. Moreover, for a detonation wave in 1-D, an adaptive mesh that uses coarser resolution around the sonic point has a very small effect on the detonation speed.

For experiments, we note that limitations on temporal resolution and uncertainty in measurements of profiles, such as velocity from VISAR or PDV probes, have a similar effect to numerical smearing of the sonic point. This gives rise to a significant uncertainty in determining

the sonic point, especially for an HE with a second slow reaction. Hence, an uncertainty in the CJ state at the end of the detonation wave which is needed to calibrate the products equation of state.

To put the numerical resolution and accuracy in perspective, PBXs are heterogeneous explosives. The spatial scale of inhomogeneities due to the grain size is typically on the order of 0.01 to 0.1 mm. The accuracy of available data to calibrate HE models is no better than a few tenths of per cent. The simulations report here are within this accuracy and use a somewhat finer cell size than the spatial inhomogeneities.

The xRage code uses operator splitting for the reactive source terms. Hence, the convergence rate is at best first order. Additional numerical errors result from interpolation of products and reactants tabular EOS for computing the P-T equilibrium EOS for partly burn HE. To achieve significantly higher accuracy would require much finer meshes for both the computational grid and the EOS tables. Even then the accuracy would be limited by numerical fluctuations in the detected shock pressure needed for the burn rate of the SURF model.

References

- W. Fickett and W. C. Davis. Detonation. Univ. of Calif. Press, 1979. 2
- E. L. Lee and C. M. Tarver. Phenomenological model of shock initiation in heterogeneous explosives. *Phys. Fluids*, 23:2362–272, 1980. 2
- R. Menikoff. Effect of resolution on propagating detonation wave. Technical Report LA-UR-14-25140, Los Alamos National Laboratory, 2014. URL http://dx.doi.org/10.2172/1136940.
- R. Menikoff. Detonation wave profile. Technical Report LA-UR-15-29498, Los Alamos National Lab., 2015. URL http://www.osti.gov/scitech/servlets/purl/1229720. 2
- R. Menikoff. Shock detector for SURF model. Technical Report LA-UR-16-20116, Los Alamos National Lab., 2016. URL http://www.osti.gov/scitech/servlets/purl/1234496. 2, 13
- R. Menikoff and M. S. Shaw. Reactive burn models and ignition & growth concept. *EPJ Web of Conferences*, 10, 2010. doi: 10.1051/epjconf/20101000003. URL http://www.epj-conferences.org/articles/epjconf/pdf/2010/09/epjconf_nmh2010_00003.pdf. 2
- R. Menikoff and M. S. Shaw. The SURF model and the curvature effect for PBX 9502. Combustion Theory And Modelling, pages 1140–1169, 2012. doi: 10.1080/13647830.2012.713994.